IEEE Access
Multidisciplinary | Rapid Review | Open Access Journal

Received October 22, 2017, accepted November 28, 2017, date of publication December 6, 2017, date of current version March 13, 2018.

*Digital Object Identifier 10.1109/ACCESS.2017.2780278*

# A Hybrid Kalman Filtering Approach Based on Federated Framework for Gas Turbine Engine Health Monitoring

**FENG LU[1], YIHUAN HUANG[2], JINQUAN HUANG[2], AND XIAOJIE QIU[2]**

[1]Jiangsu Province Key Laboratory of Aerospace Power Systems, Nanjing University of Aeronautics and Astronautics, Nanjing 210016, China
[2]Aviation Motor Control System Institute, Aviation Industry Corporation of China, Wuxi 214063, China

Corresponding authors: Feng Lu (lufengnuaa@126.com) and Jinquan Huang (jhuang@nuaa.edu.cn)

This work was supported in part by the National Nature Science Foundation of China under Grant 61304113 and in part by the China Outstanding Postdoctoral Science Foundation under Grant 2015T80552.

**ABSTRACT** The Kalman filter (KF) is the most common state estimation method for gas turbine health monitoring, and it runs in the centralized architecture. However, health estimation cannot be achieved by the KF-based method as sensor fault occurs, and malfunction of the central monitoring unit will unavoidably result to the termination of the diagnosis task. For these purposes, this paper develops a novel hybrid federated KF approach from the previous achievements. The hybrid KF consists of a bank of local filters and one master filter, and the federated filtering structure and asynchronous fusion mechanism are designed. Both the linearized KF and extended KF are employed as the local filters based on the linear correlation of thermodynamic parameters. The local state estimates and covariance are yielded in parallel, and then integrated in a master filter to produce global state estimate. The proposed methodology is evaluated and compared with the general federated KFs in terms of estimation accuracy, computational efforts, and robustness to sensor fault in the application of gas turbine health monitoring. The result shows that the hybrid KF is the best balance off the involved performance, and confirms our viewpoints in this paper.

**INDEX TERMS** Gas turbine, health monitoring, Kalman filter, asynchronous fusion, sensor fault tolerance.

## I. INTRODUCTION

Gas turbine engine is the key mechanical system to supply aircraft power, and its reliability is crucial for flight safety. Gradual deterioration of gas turbine performance is unavoidable during the course of its lifetime, and it is mainly caused by erosion and fouling of major gas path components [1], [2]. The foreign/domestic object damages result in performance degradation rapidly during its operation, and they are recognized as abrupt performance faults. Generally speaking, the variations of component efficiencies and flow capacities are employed to depict these performance anomalies, and so-called health parameters [3]. Health parameters contain important information of engine performance condition, which guide the maintenance schedule to safe operation and reduced costs [4].

Since health parameters can't be measured from the engine directly, lots of approaches have been studied in the past decades, such as weighted least squares, Kaman filters [5], [6], stochastic modeling [7], [8], neural networks [9], expert systems and genetic algorithms [10]–[12]. The KF-based methods seem to be the widely used one, and variants of the KFs are concerned including the LKF, the EKF, the UKF (Unscented KF) and the CKF (Cubature KF). The LKF is usually applied to estimate state of linear system and the rest KFs are the extension of LKF to nonlinear applications. The EKF, UKF and CKF produce similar health estimation accuracy and evidently outperform the LKF due to the mild nonlinearity of gas turbine [13]. When it comes to computational load, the EKF requires an order of magnitude higher than the LKF. The UKF and CKF have the same order of computational efforts, and yet both require another order of magnitude higher than the EKF. Thus, the LKF is the best candidate with regard to computational efforts, and EKF seems to be the best balance-off in gas turbine health monitoring.

The conventional linear and nonlinear KFs both run in a centralized architecture, and all sensor measurements are processed at a central processor. This centralized structure of

the KFs is simple, but the computational load will increase greatly with gas turbine engine complexity, in-flight tasks and estimated state parameters increase. In addition, it has more opportunity for the occurrence of sensor fault as more sensors used in harsh working condition. Decentralized filtering technology was exploited for multi-sensor systems [14], and federated KF proposed by Carlson is one of the most well-known examples in decentralized linear filtering structure [15]. The computational loads are assigned by several LKF individuals in the federated KF approach.

Similar to the centralized architecture, some kinds of nonlinear federated KF are developed from the linearized one in the recent years, such as the FEKF (federated EKF) and FUKF (federated UKF) algorithms. The FEKF is presented to improve the accuracy and reliability of vehicle position estimation [16], and the FUKF utilized to estimate navigation parameters [17]. The FUKF contains a fault detection and isolation module, and the navigation system will not break down even if one sensor faulty. Other researches prove the superiority of federated filtering structure in terms of high estimation precision and high fault tolerance in the application of multi-sensor integrated navigation system [18]–[20]. In a word, the progress on the federated filters achieved above relies on the same local filters, while the integration of different kinds of local filters is not referred.

Motivated by taking the advantage of federated filtering method, this paper proposes a novel hybrid Kalman filtering methodology by the combination of linear and nonlinear local KFs, and then applies it for aero-engine health monitoring in decentralized filtering architecture. The available sensor measurements for health estimation are partitioned into several sensor subsets, and every subset is related to one local filter. The LKF and EKF are used to form local filters, and the parameters of which depends on linear parameters correlation. These local filters independently collect the sensed data, and synchronously cope with the data in the field. One master filter receives and integrates all sensor-based estimates from the local filters to generate the global state estimate on the top of decentralized structure. The global state and covariance are weighted and feedback to different kinds of local filters. The equivalence of the HKF and general EKF for state estimation is mathematically proved with the least square errors based on an information-sharing principle. The simulation results of engine health monitoring demonstrate the superiority of the proposed methodology in both total computational effort and robustness to sensor faults.

The remainder of this paper is organized as follows. Section 2 gives aero-engine gas path health description and a review of centralized Kalman filters. In Section 3, a systematic framework of the HKF, and its fault diagnosis and isolation (FDI) mechanism are developed in detail. Simulation results based on a nonlinear turbofan model is presented in Section 4, along with some comparisons between the proposed HKF and general federated KFs. The conclusion is drawn in Section 5.

## II. GAS PATH HEALTH USING CENTRALIZED KALMAN FILTERS

### A. GAS PATH HEALTH DESCRIPTION

In this paper, a two-spool turbofan engine is studied, which is recognized as the most important aircraft propulsion systems. The main components of the engine consist of inlet, fan, compressor, bypass, combustor, HPT (high pressure turbine), LPT (low pressure turbine), mixer and nozzle. The airflow is supplied to the fan from inlet, and then separates into two streams: one stream passes through the engine core path, and the other passes through the annular bypass duct. It is driven into the combustor after through compressor. Fuel is injected into the combustor and burned to produce hot gas to drive turbines. The fan is driven by the LPT and the compressor by the HPT. Finally, the mixed gas from LPT and bypass exhausts discharge through nozzle [11].

On the basis of air flow mass, power and momentum conservation laws, a nonlinear mathematical model is established to describe the turbofan engine. The thermodynamic relationship of engine model is expressed as follows

$$\begin{aligned} \boldsymbol{x}_{0,k+1} &= \boldsymbol{x}_{0,k} + \boldsymbol{w}_{0,k} \\ \boldsymbol{y}_k &= g(\boldsymbol{x}_{0,k}, \boldsymbol{u}_k) + \boldsymbol{v}_{0,k} \end{aligned} \tag{1}$$

where $k$ is a discrete time index, $\boldsymbol{x}_0$ is the original state vector and $\boldsymbol{u}$ is the control vector. The engine output $\boldsymbol{y}$ is observed by a set of available sensor measurements, and the function $\boldsymbol{g}()$ represent the engine operating equation. The process noise term $\boldsymbol{w}_{0,k}$ with covariance matrix $\boldsymbol{Q}_0$ denotes the system inaccuracy, and measurement noise term $\boldsymbol{v}_{0,k}$ with its covariance $\boldsymbol{R}_0$ denotes the measurement inaccuracy. The original state variables contain low-pressure spool speed $N_L$ and high-pressure spool speed $N_H$. The elements of control vector in the model are fuel flow $W_f$ and nozzle area $A_8$, which determine the engine operating point. The measurements are $N_L$, $N_H$, fan outlet temperature $T_{22}$, fan outlet pressure $P_{22}$, compressor outlet temperature $T_3$, compressor outlet pressure $P_3$, HPT outlet temperature $T_{43}$, HPT outlet pressure $P_{43}$, LPT outlet temperature $T_6$ and LPT outlet pressure $P_6$.

Gas path abnormal incidents of the turbofan engine include gradual performance deterioration and abrupt gas path fault, and health parameters representing the health condition of turbofan engine are denoted as vector $\boldsymbol{h}$. In this study, the efficiencies and flow capacities of four major rotating components, like fan, compressor, HPT and LPT, are defined below form the health parameter vector

$$SE_i = \frac{E_{i,real}}{E_{i,nor}}, \quad SW_i = \frac{W_{i,real}}{W_{i,nor}} \quad i = 1, \cdots, 4 \tag{2}$$

where the subscript $i$ from 1 to 4 is successively fan, compressor, HPT and LPT. The subscript *real* denotes the real efficiency $SE$ and flow capacity $SW$ values, and *nor* is their design values. The health parameter vector can be written as $\boldsymbol{h} = [SE_1, SW_1, SE_2, SW_2, SE_3, SW_3, SE_4, SW_4]^{\mathrm{T}}$. Both the engine performance gradual deterioration and component

abrupt deviations can result in health parameters variations. Health parameters of interest are unmeasured directly in the plants, while their variations will result in the measurement changes. Thus, the sensor measurements are employed to calculated health parameters by state estimation algorithms to obtain the engine health condition.

### B. CENTRALIZED KALMAN FILTERS

The LKF is an optimal state estimator with the advantages of real-time computation and resistance to measurement noise. The health parameters are supplemented to the spool speeds to form the augmented state $\boldsymbol{x} = [N_L, N_H, \boldsymbol{h}^{\mathrm{T}}]^{\mathrm{T}}$ to be estimated by the LKF. The LKF-based approach for health monitoring has a recursive and predictor-corrector structure. The prior values of health parameters are generated through engine state transition equation, and then the residuals between the actual measurements and estimated ones from the measurement equation are acquired to correct the predicted health parameters [21], [22].

State variable models (SVM) at several steady operating points are established before the use of the LKF. The actual engine model in whole operating range is described by a piecewise linear representation based on the SVMs. The centralized LKF includes time update and measurement update that are separately given in Eq. (3) and Eq. (4).

$$\begin{aligned} \hat{\boldsymbol{x}}_{k|k-1} &= \hat{\boldsymbol{x}}_{k-1} \\ \boldsymbol{P}_{k|k-1} &= \boldsymbol{P}_{k-1} + \boldsymbol{Q}_{k-1} \end{aligned} \tag{3}$$

$$\begin{aligned} \boldsymbol{K}_k &= \boldsymbol{P}_{k|k-1}\boldsymbol{C}_k^T(\boldsymbol{C}_k\boldsymbol{P}_{k|k-1}\boldsymbol{C}_k^T + \boldsymbol{R}_k)^{-1} \\ \hat{\boldsymbol{x}}_k &= \hat{\boldsymbol{x}}_{k|k-1} + \boldsymbol{K}_k(\boldsymbol{y}_k - \boldsymbol{C}_k\hat{\boldsymbol{x}}_{k|k-1} - \boldsymbol{D}_k\boldsymbol{u}_k) \\ \boldsymbol{P}_k &= (\boldsymbol{I} - \boldsymbol{K}_k\boldsymbol{C}_k)\boldsymbol{P}_{k|k-1} \end{aligned} \tag{4}$$

where $\boldsymbol{C}_k$, $\boldsymbol{D}_k$ are the coefficient matrices of the SVM at time $k$, and the detailed calculation of these matrices can be referred to [23]. These matrices are obtained off-line and updated with steady operating point. An identity matrix $\boldsymbol{I}$ is with appropriate dimension, $\boldsymbol{K}_k$ is Kalman gain and $\boldsymbol{P}_{\mathbf{k}}$ is the state estimate covariance matrix computed at time $k$. The estimation performance of the LKF varies with the distance from the actual operating point to steady operating point. The larger distance from the steady operating point, the more estimation errors is produced.

The EKF is an important state estimator for nonlinear system, where the SVM is not necessary. The less model linearization errors are introduced, and affect to the state estimation accuracy in the EKF. It utilizes a first order linearization to propagate state mean and covariance, and contains time update and measurement update [24]. Time update equation of the EKF is the same as the LKF given in Eq. (3), and measurement update formulation is presented in Eq. (5). The coefficient matrices $\boldsymbol{C}$ in the EKF is calculated on-line and update at each step in the engine trajectory. Compared to LKF, the EKF has better estimation accuracy but more computational effort paid. Most computational effort is consumed on Jacobian calculation to obtain the coefficient matrices at each step.

$$\begin{aligned} \boldsymbol{K}_k &= \boldsymbol{P}_{k|k-1}\boldsymbol{C}_k^T(\boldsymbol{C}_k\boldsymbol{P}_{k|k-1}\boldsymbol{C}_k^T + \boldsymbol{R}_k)^{-1} \\ \hat{\boldsymbol{x}}_k &= \hat{\boldsymbol{x}}_{k|k-1} + \boldsymbol{K}_k[\boldsymbol{y}_k - g(\hat{\boldsymbol{x}}_{k|k-1}, \boldsymbol{u}_k)] \\ \boldsymbol{P}_k &= (\boldsymbol{I} - \boldsymbol{K}_k\boldsymbol{C}_k)\boldsymbol{P}_{k|k-1} \end{aligned} \tag{5}$$

where

$$\boldsymbol{C}_k = \frac{\partial g(\hat{\boldsymbol{x}}_k, \boldsymbol{u}_k)}{\partial \boldsymbol{x}}\Big|_{\boldsymbol{x}=\hat{\boldsymbol{x}}_{k|k-1}} \tag{6}$$

Both the LKF and EKF algorithms for engine health estimation are organized in a centralized architecture. All sensed data are fed into one central processor for state estimation. Since each measurement is identically processed by one central filter at a time, this filter experiences heavy computational loads as the number of system parameters increases. Besides, the general Kalman filter can't make sense of sensor fault, and the wrong sensed data will lead to mistakes of health estimation. In the next section, we will combine the LKF and EKF to advance a novel hybrid Kalman filter in the decentralized architecture for engine health monitoring.

## III. HYBRID FEDERATED KALMAN FILTER FOR ENGINE HEALTH ESTIMATION

### A. DESIGN OF THE HYBRID FEDERATED KALMAN FILTER

Hybrid federated Kalman filter is developed based on the integration of KFs and information fusion theory. In the application of gas turbine health monitoring, the measurements for state estimation are optimally selected and divided into two teams by linear correlation analysis [25]. The estimation errors of health parameters from the linear model and nonlinear model are used to represent linear correlation of the parameters [26], [27]. The sensor subsets with less linearity are stream to the local EKFs, while the remaining sensor subsets to the local LKFs to estimate health parameters. The measurements in each sensor subset for estimation are different, and health parameters to be estimated are the same in local filters, namely, $SE_1$, $SW_1$, $SE_2$, $SW_2$, $SE_3$, $SW_3$, $SE_4$ and $SW_4$.

On the other hand, engine gas path sensor layout is taken into account for the assignment of sensor subsets related to local filters in the distributed architecture. A large number of sensed data are collected and transmitted to a single processing center, and it results in an overhead to the communication bandwidth as the number of sensors increase. Some measurement transmissions to the processing center are practically remotely and hard or even impossible. The sensor neighborhood along the engine gas path is considered to form the sensor subsets in the decentralized KFs. The processed local sensor information is delivered to the processing center by the bus, and it reduces the transmission load and interference. The HKF modeling parameters are determined by the integration of linear correlation analysis and engine sensor layout.

The HKF for the engine health monitoring is designed and mainly includes three stages. Firstly, the local LKFs and EKFs perform in parallel to obtain local estimates from their own sensor subsets. Secondly, all local estimates of

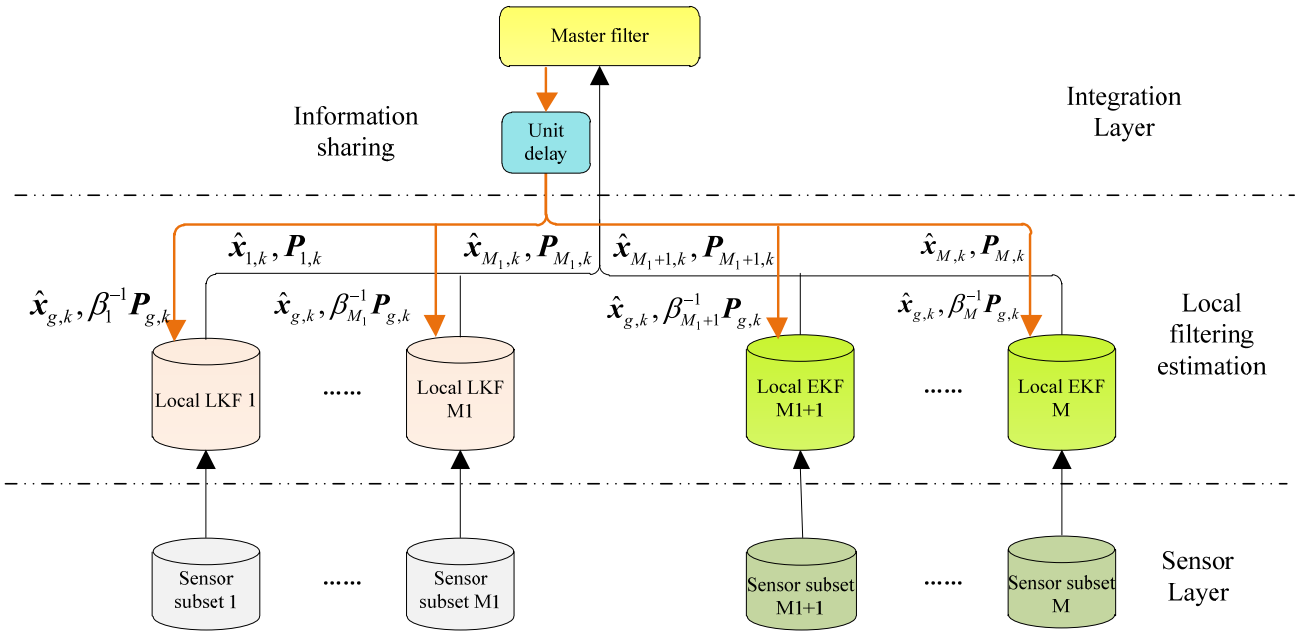


**FIGURE 1.** The framework of proposed HKF for engine health monitoring.

health parameters are sent to a master filter in the centralized processor, where a global state estimate is reached. Thirdly, the global health state and covariance are fed back to local LKFs and EKFs with an information-sharing strategy for next step calculation. Assume that there are $M_1$ local LKFs and $M_2$ local EKFs in the decentralized filtering architecture, then the HKF has totally $M = M_1 + M_2$ local filters. The detailed procedure of the HKF is summarized as follows.

*Step 1 (Initialization):* Given the initial global state vector $\hat{\boldsymbol{x}}_{g,0}$, estimation error covariance $\boldsymbol{P}_{g,0}$, and process noise covariance $\boldsymbol{Q}_0$ with appropriate dimension in the master filter. Then initialize the modeling parameters of local filters

$$\hat{\boldsymbol{x}}_{i,0}=\hat{\boldsymbol{x}}_{g,0} \quad \boldsymbol{P}_{i,0}=\beta_i^{-1}\boldsymbol{P}_{g,0} \quad \boldsymbol{Q}_{i,0}=\beta_i^{-1}\boldsymbol{Q}_0 \quad i=1,\cdots,M \tag{7}$$

where $\beta_i$ is the information-sharing factor, and it follows $\sum_{i=1}^{M}\beta_i = 1$. This factor $\beta_i$ is usually a constant, and equal to average coefficient. It is set by $\beta_i = 1/M$ in this paper.

*Step 2 (Time Update and Measurement Update in the Local Filters):* The time update and measurement update process are carried out independently in local filters at each iteration step. The local estimates of the local LKFs are computed by the Eq. (3) and Eq. (4), and the local estimates of the local EKFs computed by the Eq. (5) and Eq. (6).

*Step 3 (Local Estimates Fusion in the Master Filter):* The local estimates $\hat{\boldsymbol{x}}_{i,k}$ and $\boldsymbol{P}_{i,k}$ are transmitted to synthetize in the master filter. The optimal global state estimate $\hat{\boldsymbol{x}}_{g,k}$ and error covariance $\boldsymbol{P}_{g,k}$ are obtained by the following additive information fusion

$$\boldsymbol{P}_{g,k}^{-1} = \sum_{i=1}^{M}\boldsymbol{P}_{i,k}^{-1} \tag{8}$$

$$\hat{\boldsymbol{x}}_{g,k} = \boldsymbol{P}_{g,k}\sum_{i=1}^{M}\left(\boldsymbol{P}_{i,k}^{-1}\hat{\boldsymbol{x}}_{i,k}\right) \tag{9}$$

where $\boldsymbol{x}_{\mathbf{i},\mathbf{k}}$ is the $i$-th local state vector at time $k$ with the local process noise covariance $\boldsymbol{Q}_{\mathbf{i},\mathbf{k}}$, and its state estimate covariance matrix is $\boldsymbol{P}_{\mathbf{i},\mathbf{k}}$.

*Step 4 (Global Information Feedback):* The global state and covariance generated by the master filter are fed back to local filters for the next step of recursive calculation. The information-sharing strategy follows as $\hat{\boldsymbol{x}}_{i,k} = \hat{\boldsymbol{x}}_{g,k}$, $\boldsymbol{P}_{i,k} = \beta_i^{-1}\boldsymbol{P}_{g,k}$, $\boldsymbol{Q}_{i,k}=\beta_i^{-1}\boldsymbol{Q}_k$ $(i=1,\cdots,M)$.

For step $k+1$, the calculated values of state and covariance delay a time index, and steps (2)-(4) are repeated. The block diagram of the HKF algorithm for engine health monitoring is shown in Figure 1.

Compared to the centralized framework, state estimation task in HKF is decomposed from a KF in a processing center into several LKFs and EKFs in the field, and one master filter in the center. In other words, the master filter and local KFs share the computation burden of the general KF together, which avoids the overload in a single processor. Although the estimates of HKF are distributed over a network, the global estimate is optimal and conservatively equivalent to that of the centralized EKF.

### B. EQUIVALENCE ANALYSIS OF THE HKF

The mathematical equivalence of the HKF and centralized EKF is presented in this section. Provided that the two

KFs have the same initial parameters, the equivalent conclusion can be reached as the time update and measurement update expressions of the HKF and EKF are mathematically consistent.

Assume five sensor subsets are designed for engine health estimation, and they are two local LKFs and three local EKFs. The $i$-th local system can be described by the following state transition equation and measurement equation

$$\boldsymbol{x}_{k+1} = \boldsymbol{x}_k + \boldsymbol{w}_k \tag{10}$$

$$\boldsymbol{y}_{i,k} = \boldsymbol{C}_{i,k}\boldsymbol{x}_k + \boldsymbol{D}_{i,k}\boldsymbol{u}_k + \boldsymbol{v}_{i,k} \quad i = 1, 2 \tag{11}$$

$$\boldsymbol{y}_{i,k} = g_i(\boldsymbol{x}_k, \boldsymbol{u}_k) + \boldsymbol{v}_{i,k} \quad i = 3, 4, 5 \tag{12}$$

where $\boldsymbol{y}_{i,k}$ is the measured vector from the $i$-th sensor subsystem at time $k$, and its measurement noise term $\boldsymbol{v}_{i,k}$ with its covariance $\boldsymbol{R}_{i,k}$. $\boldsymbol{C}_{i,k}$, $\boldsymbol{D}_{i,k}$ are the coefficient matrices of the $i$-th subsystem at time $k$. The linear measurement equation Eq. (11) is a special form of nonlinear function, and it is obtained by Taylor Expansion.

The combined measurement expressions of the hybrid system in the distributed framework are

$$\begin{aligned} \boldsymbol{y}_k &= [\boldsymbol{y}_{1,k}^T, \boldsymbol{y}_{2,k}^T, \cdots \boldsymbol{y}_{5,k}^T]^T \\ \boldsymbol{v}_k &= [\boldsymbol{v}_{1,k}^T, \boldsymbol{v}_{2,k}^T, \cdots, \boldsymbol{v}_{5,k}^T]^T \\ \boldsymbol{R}_k &= diag(\boldsymbol{R}_{1,k}, \boldsymbol{R}_{2,k}, \cdots, \boldsymbol{R}_{5,k}) \end{aligned} \tag{13}$$

In the fusion module, the EKF treats measurement data from each sensor subset identically to obtain the state estimates. It runs time update equations at time $k$, then the EKF performs measurement update process.

$$\begin{aligned} \hat{\boldsymbol{x}}_{k|k-1} &= \hat{\boldsymbol{x}}_{k-1} \\ \boldsymbol{P}_{k|k-1} &= \boldsymbol{P}_{k-1} + \boldsymbol{Q}_k \end{aligned} \tag{14}$$

For more convenient derivation of equivalence, measurement update of the EKF is expressed by information filtering equations, and it mainly contains covariance inverse $\boldsymbol{P}_k^{-1}$ and information state estimate $\boldsymbol{P}_k^{-1}\hat{\boldsymbol{x}}_k$. Previous publication reveals that two filters are equivalent only these two terms of the EKF and HKF consistent [24].

$$\begin{aligned} \boldsymbol{P}_k^{-1} &= \boldsymbol{P}_{k|k-1}^{-1} + \boldsymbol{C}_k^T\boldsymbol{R}_k^{-1}\boldsymbol{C}_k \\ \boldsymbol{P}_k^{-1}\hat{\boldsymbol{x}}_k &= \boldsymbol{P}_{k|k-1}^{-1}\hat{\boldsymbol{x}}_{k|k-1} + \boldsymbol{C}_k^T\boldsymbol{R}_k^{-1} \\ &\quad \times [\boldsymbol{y}_k - g(\hat{\boldsymbol{x}}_{k|k-1}, \boldsymbol{u}_k) + \boldsymbol{C}_k\hat{\boldsymbol{x}}_{k|k-1}] \end{aligned} \tag{15}$$

Since each local filter of the HKF has the same state transition equation, and they are also the same as the EKF. According to the information allocation equations $\boldsymbol{Q}_{i,k-1} = \beta_i^{-1}\boldsymbol{Q}_{k-1}$, $\boldsymbol{P}_{i,k-1} = \beta_i^{-1}\boldsymbol{P}_{g,k-1}$, the priori covariance matrix of the $i$-th local filter can be written as

$$\begin{aligned} \boldsymbol{P}_{i,k|k-1} &= \boldsymbol{P}_{i,k-1} + \boldsymbol{Q}_{i,k} = \beta_i^{-1}\boldsymbol{P}_{g,k-1} + \beta_i^{-1}\boldsymbol{Q}_k \\ &= \beta_i^{-1}\left(\boldsymbol{P}_{g,k-1} + \boldsymbol{Q}_k\right) = \beta_i^{-1}\boldsymbol{P}_{g,k|k-1} \end{aligned} \tag{16}$$

Then the global priori covariance matrix of the HKF is calculated by

$$\begin{aligned} \boldsymbol{P}_{g,k|k-1}^{-1} &= \sum_{i=1}^{2}\boldsymbol{P}_{i,k|k-1}^{-1} + \sum_{i=3}^{5}\boldsymbol{P}_{i,k|k-1}^{-1} \\ &= \sum_{i=1}^{2}\left(\boldsymbol{P}_{i,k-1}+\boldsymbol{Q}_{i,k}\right)^{-1} + \sum_{i=3}^{5}\left(\boldsymbol{P}_{i,k-1}+\boldsymbol{Q}_{i,k}\right)^{-1} \\ &= \sum_{i=1}^{5}\left(\boldsymbol{P}_{i,k-1} + \boldsymbol{Q}_{i,k}\right)^{-1} \\ &= \sum_{i=1}^{5}\left(\beta_i^{-1}\boldsymbol{P}_{g,k-1} + \beta_i^{-1}\boldsymbol{Q}_k\right)^{-1} \\ &= \sum_{i=1}^{5}\beta_i\left(\boldsymbol{P}_{g,k-1}+\boldsymbol{Q}_k\right)^{-1} = \left(\boldsymbol{P}_{g,k-1}+\boldsymbol{Q}_k\right)^{-1} \end{aligned} \tag{17}$$

Substituting Eq. (16) into information fusion strategy Eq. (6), and it yields the global priori HKF state vector

$$\begin{aligned} &\hat{\boldsymbol{x}}_{g,k|k-1} \\ &= \boldsymbol{P}_{g,k|k-1}\left\{\sum_{i=1}^{2}\left(\boldsymbol{P}_{i,k|k-1}^{-1}\hat{\boldsymbol{x}}_{i,k|k-1}\right) + \sum_{i=3}^{5}\left(\boldsymbol{P}_{i,k|k-1}^{-1}\hat{\boldsymbol{x}}_{i,k|k-1}\right)\right\} \\ &= \boldsymbol{P}_{g,k|k-1}\left\{\sum_{i=1}^{2}\left(\beta_i\boldsymbol{P}_{g,k|k-1}^{-1}\hat{\boldsymbol{x}}_{i,k|k-1}\right)\right. \\ &\qquad \left. + \sum_{i=3}^{5}\left(\beta_i\boldsymbol{P}_{g,k|k-1}^{-1}\hat{\boldsymbol{x}}_{i,k|k-1}\right)\right\} \\ &= \sum_{i=1}^{5}\beta_i\left(\hat{\boldsymbol{x}}_{i,k-1}\right) = \sum_{i=1}^{5}\beta_i\left(\hat{\boldsymbol{x}}_{g,k-1}\right) = \hat{\boldsymbol{x}}_{g,k-1} \end{aligned} \tag{18}$$

As can be seen from Eq. (17) and Eq. (18), the global priori state vector and covariance matrix of the HKF are identical to those of the centralized EKF in Eq. (14). Hence, we have the equivalence of time update expression between the HKF and centralized EKF.

When the measurement update is concerned, the global posteriori covariance of HKF is calculated by

$$\begin{aligned} \boldsymbol{P}_{g,k}^{-1} &= \sum_{i=1}^{2}\boldsymbol{P}_{i,k}^{-1} + \sum_{i=3}^{5}\boldsymbol{P}_{i,k}^{-1} = \sum_{i=1}^{2}\left(\boldsymbol{P}_{i,k|k-1}^{-1} + \boldsymbol{C}_{i,k}^T\boldsymbol{R}_{i,k}^{-1}\boldsymbol{C}_{i,k}\right) \\ &\quad + \sum_{i=3}^{5}\left(\boldsymbol{P}_{i,k|k-1}^{-1} + \boldsymbol{C}_{i,k}^T\boldsymbol{R}_{i,k}^{-1}\boldsymbol{C}_{i,k}\right) \\ &= \sum_{i=1}^{5}\left(\boldsymbol{P}_{i,k|k-1}^{-1} + \boldsymbol{C}_{i,k}^T\boldsymbol{R}_{i,k}^{-1}\boldsymbol{C}_{i,k}\right) \\ &= \sum_{i=1}^{5}\boldsymbol{P}_{i,k|k-1}^{-1} + \sum_{i=1}^{5}\boldsymbol{C}_{i,k}^T\boldsymbol{R}_{i,k}^{-1}\boldsymbol{C}_{i,k} \\ &= \sum_{i=1}^{5}\beta_i\boldsymbol{P}_{g,k|k-1}^{-1} + \left[\boldsymbol{C}_{1,k}^T, \cdots, \boldsymbol{C}_{5,k}^T\right] \\ &\quad \times diag\left[\boldsymbol{R}_{1,k}^{-1}, \cdots, \boldsymbol{R}_{5,k}^{-1}\right] \times \left[\boldsymbol{C}_{1,k}^T, \cdots, \boldsymbol{C}_{5,k}^T\right]^T \\ &= \boldsymbol{P}_{g,k|k-1}^{-1} + \boldsymbol{C}_k^T\boldsymbol{R}_k^{-1}\boldsymbol{C}_k \end{aligned} \tag{19}$$

Then the global posteriori state vector of HKF can be computed by

$$\begin{aligned}\boldsymbol{P}_{g,k}^{-1}\hat{\boldsymbol{x}}_{g,k} &= \sum_{i=1}^{2}\left(\boldsymbol{P}_{i,k}^{-1}\hat{\boldsymbol{x}}_{i,k}\right)+\sum_{i=3}^{5}\left(\boldsymbol{P}_{i,k}^{-1}\hat{\boldsymbol{x}}_{i,k}\right)\\ &= \sum_{i=1}^{2}\left\{\boldsymbol{P}_{i,k|k-1}^{-1}\hat{\boldsymbol{x}}_{i,k|k-1}+\boldsymbol{C}_{i,k}^{T}\boldsymbol{R}_{i,k}^{-1}(\boldsymbol{y}_{i,k}-\boldsymbol{D}_{i,k}\boldsymbol{u}_{k})\right\}\\ &\quad+\sum_{i=3}^{5}\left\{\boldsymbol{P}_{i,k|k-1}^{-1}\hat{\boldsymbol{x}}_{i,k|k-1}+\boldsymbol{C}_{i,k}^{T}\boldsymbol{R}_{i,k}^{-1}\right.\\ &\quad\left.\times\left[\boldsymbol{y}_{i,k}-\boldsymbol{g}_{i}\left(\hat{\boldsymbol{x}}_{i,k|k-1},\boldsymbol{u}_{k}\right)+\boldsymbol{C}_{i,k}\hat{\boldsymbol{x}}_{i,k|k-1}\right]\right\} \quad (20)\end{aligned}$$

Since the coefficient matrices $\boldsymbol{C}_{i,k}$ and $\boldsymbol{D}_{i,k}$ are obtained from the measurement function $\boldsymbol{g}_i()$, the linear item in Eq. (20) can be rewritten by

$$\boldsymbol{y}_{i,k}-\boldsymbol{D}_{i,k}\boldsymbol{u}_{k}=\boldsymbol{y}_{i,k}-\boldsymbol{g}_{i}\left(\hat{\boldsymbol{x}}_{i,k|k-1},\boldsymbol{u}_{k}\right)+\boldsymbol{C}_{i,k}\hat{\boldsymbol{x}}_{i,k|k-1}\quad i=1,2 \quad (21)$$

On the other hand, since the global state is fully feedback to the local filters, namely $\hat{\boldsymbol{x}}_{i,k|k-1}=\hat{\boldsymbol{x}}_{g,k|k-1}$. The global posteriori state vector of HKF can be finally given as

$$\begin{aligned}\boldsymbol{P}_{g,k}^{-1}\hat{\boldsymbol{x}}_{g,k} &= \sum_{i=1}^{5}\left\{\boldsymbol{P}_{i,k|k-1}^{-1}\hat{\boldsymbol{x}}_{i,k|k-1}+\boldsymbol{C}_{i,k}^{T}\boldsymbol{R}_{i,k}^{-1}\right.\\ &\quad\left.\times\left[\boldsymbol{y}_{i,k}-\boldsymbol{g}\left(\hat{\boldsymbol{x}}_{i,k|k-1},\boldsymbol{u}_{k}\right)+\boldsymbol{C}_{i,k}\hat{\boldsymbol{x}}_{i,k|k-1}\right]\right\}\\ &= \sum_{i=1}^{5}\left\{\boldsymbol{P}_{i,k|k-1}^{-1}\hat{\boldsymbol{x}}_{g,k|k-1}+\boldsymbol{C}_{i,k}^{T}\boldsymbol{R}_{i,k}^{-1}\right.\\ &\quad\left.\times\left[\boldsymbol{y}_{i,k}-\boldsymbol{g}_{i}\left(\hat{\boldsymbol{x}}_{g,k|k-1},\boldsymbol{u}_{k}\right)+\boldsymbol{C}_{i,k}\hat{\boldsymbol{x}}_{g,k|k-1}\right]\right\}\\ &= \sum_{i=1}^{5}\boldsymbol{P}_{i,k|k-1}^{-1}\hat{\boldsymbol{x}}_{g,k|k-1}+\sum_{i=1}^{5}\boldsymbol{C}_{i,k}^{T}\boldsymbol{R}_{i,k}^{-1}\boldsymbol{y}_{i,k}\\ &\quad-\sum_{i=1}^{5}\boldsymbol{C}_{i,k}^{T}\boldsymbol{R}_{i,k}^{-1}\boldsymbol{g}_{i}\left(\hat{\boldsymbol{x}}_{g,k|k-1},\boldsymbol{u}_{k}\right)\\ &\quad+\sum_{i=1}^{5}\boldsymbol{C}_{i,k}^{T}\boldsymbol{R}_{i,k}^{-1}\boldsymbol{C}_{i,k}\hat{\boldsymbol{x}}_{g,k|k-1}\\ &= \sum_{i=1}^{5}\beta_{i}\boldsymbol{P}_{g,k|k-1}^{-1}\hat{\boldsymbol{x}}_{g,k|k-1}+\left[\boldsymbol{C}_{1,k}^{T},\cdots,\boldsymbol{C}_{5,k}^{T}\right]\\ &\quad\times diag\left[\boldsymbol{R}_{1,k}^{-1},\cdots,\boldsymbol{R}_{5,k}^{-1}\right]\times\left[\boldsymbol{y}_{1,k}^{T},\cdots,\boldsymbol{y}_{5,k}^{T}\right]^{T}\\ &\quad-\left[\boldsymbol{C}_{1,k}^{T},\cdots,\boldsymbol{C}_{5,k}^{T}\right]\times diag\left[\boldsymbol{R}_{1,k}^{-1},\cdots,\boldsymbol{R}_{5,k}^{-1}\right]\\ &\quad\times\left[\boldsymbol{g}_{1}^{T}\left(\hat{\boldsymbol{x}}_{g,k|k-1},\boldsymbol{u}_{k}\right),\cdots,\boldsymbol{g}_{5}^{T}\left(\hat{\boldsymbol{x}}_{g,k|k-1},\boldsymbol{u}_{k}\right)\right]^{T}\\ &\quad+\left[\boldsymbol{C}_{1,k}^{T},\cdots,\boldsymbol{C}_{5,k}^{T}\right]\times diag\left[\boldsymbol{R}_{1,k}^{-1},\cdots,\boldsymbol{R}_{5,k}^{-1}\right]\\ &\quad\times\left[\boldsymbol{C}_{1,k}^{T},\cdots,\boldsymbol{C}_{5,k}^{T}\right]^{T}\times\hat{\boldsymbol{x}}_{g,k|k-1}\\ &= \boldsymbol{P}_{g,k|k-1}^{-1}\hat{\boldsymbol{x}}_{g,k|k-1}+\boldsymbol{C}_{k}^{T}\boldsymbol{R}_{k}^{-1}\boldsymbol{y}_{k}\\ &\quad-\boldsymbol{C}_{k}^{T}\boldsymbol{R}_{k}^{-1}\boldsymbol{g}\left(\hat{\boldsymbol{x}}_{g,k|k-1},\boldsymbol{u}_{k}\right)+\boldsymbol{C}_{k}^{T}\boldsymbol{R}_{k}^{-1}\boldsymbol{C}_{k}\hat{\boldsymbol{x}}_{g,k|k-1}\\ &= \boldsymbol{P}_{g,k|k-1}^{-1}\hat{\boldsymbol{x}}_{g,k|k-1}+\boldsymbol{C}_{k}^{T}\boldsymbol{R}_{k}^{-1}\\ &\quad\times\left[\boldsymbol{y}_{k}-\boldsymbol{g}\left(\hat{\boldsymbol{x}}_{g,k|k-1},\boldsymbol{u}_{k}\right)+\boldsymbol{C}_{k}\hat{\boldsymbol{x}}_{g,k|k-1}\right] \quad (22)\end{aligned}$$

It can be easily found from Eq. (19) and Eq. (22) that the global posteriori covariance matrix and state vector of HKF are identical to those of the EKF in Eq. (15). The measurement update consistence between the HKF and centralized EKF is likewise deduced. The proof is completed.

### C. THE FDI MECHANISM IN HKF

Both the time and measurement update are carried out independently in each local filter, and the local estimates are not immediately affected mutually at the current step. The HKF has a nature advantage in the capability of sensor fault tolerance. The FDI mechanism is inherently included in the HKF algorithm, and it relies on the consistency of the local state estimates. The variance of local estimates is regarded as the sensor fault detection index. When no sensor fault exists, all local estimates are close to the real state, and the variance of state estimates between the local individuals is small. Once a sensor fault occurs, the local estimate generated by its related local filter is polluted with faulty sensor data. This local estimate deviates from the real state and different from other estimates generated by normal local filters, and it leads to the fault detection index exceeding the fault threshold. Then faulty sensor subset can be detected, and its related local filter will be isolated from the distributed framework. Although one local filter is excluded, the measurement number is eight and no less than the estimated state count. Hence, the HKF still follows the observability of state estimator, that is to say, the engine health estimation will not be interrupted as the sensor fault happens in one subset.

The proposed HKF runs in the proposition that all local filters provide estimates to the master filter synchronously, but it is difficult to realize in engineering. The update frequencies of various sensor devices are different and the local EKF usually consumes more computational effort than local LKF. Literature [28] presented an unequal-interval federated filtering method to the problem of the output cycle inconsistency of local filters. The asynchronous fusion mechanism is introduced in the HKF, the greatest common divisor of all local output cycles is taken as the calculation cycle and the least common multiple as the fusion cycle. When one measured channel provides no information, the related local filter only carries out time updating process. Based on this asynchronous fusion mechanism, the implementation steps of the HKF are briefly summarized as follows:

(1) At the calculation cycle that only part of the local filters has measurement information.

a) The local filter with measurement information carries out time updating and measurement updating process, and the others without measurement information only carries out time updating process.

b) The master filter firstly carries out time updating process, like the local filter. Then it fuses the estimates from local filters by the Eq. (23)

$$\begin{aligned} \boldsymbol{P}_{g,k}^{-1} &= \boldsymbol{P}_{g,k|k-1}^{-1} + \sum_{i=0}^{J} (\boldsymbol{P}_{i,k}^{-1} - \boldsymbol{P}_{i,k|k-1}^{-1}) \\ \hat{\boldsymbol{x}}_{g,k} &= \boldsymbol{P}_{g,k}\{\boldsymbol{P}_{g,k|k-1}^{-1}\hat{\boldsymbol{x}}_{g,k|k-1} \\ &\quad + \sum_{i=0}^{J} (\boldsymbol{P}_{i,k}^{-1}\hat{\boldsymbol{x}}_{i,k} - \boldsymbol{P}_{i,k|k-1}^{-1}\hat{\boldsymbol{x}}_{i,k|k-1})\} \end{aligned} \quad (23)$$

where $J$ denotes the number of local filters with measurement at time $k$.

(2) At the fusion cycle that all of the local filters have the sensed measurement.

This period is ideal for the HKF to perform in accordance with the normal steps. All local filters are responsible for running time and measurement updating process, and the master filter fuses local estimates and the global state estimate is then fed back to local filters.

**TABLE 1. Gas turbine engine measurements, nominal value, and standard deviation.**

| Measurement | Acronyms | Normalized value | Standard deviation |
|---|---|---|---|
| Low pressure spool speed | $N_L$ | 1 | 0.0015 |
| High pressure spool speed | $N_H$ | 1 | 0.0015 |
| Fan outlet temperature | $T_{22}$ | 1 | 0.002 |
| Fan outlet pressure | $P_{22}$ | 1 | 0.0015 |
| HPC outlet temperature | $T_3$ | 1 | 0.002 |
| HPC outlet pressure | $P_3$ | 1 | 0.0015 |
| HPT outlet temperature | $T_{43}$ | 1 | 0.002 |
| HPT outlet pressure | $P_{43}$ | 1 | 0.0015 |
| LPT outlet temperature | $T_6$ | 1 | 0.002 |
| LPT outlet pressure | $P_6$ | 1 | 0.0015 |

## IV. SIMULATION AND ANALYSIS

The proposed HKF is evaluated by a systematical discussion for gas turbine engine health monitoring in cases of abrupt and gradual performance deterioration. The computation burden and robustness to sensor faults are compared and discussed. In the simulations, the actual engine is replaced by a component level model (CLM) with sampling rate of 20 ms. The CLM is coded with C language and packaged by dynamic link library in Matlab environment [29]. The PC hardware used for simulations is configured as follows: CPU i3-550 @ 3.20 GHz and RAM 4 GB. The normalized values and standard deviations of sensor measurements are listed in Table 1. Gaussian noise $\boldsymbol{v}$ with magnitude specified in Table 1 is added to the measured values [30], and the independent system noise and measured noise separately follow $\omega \sim N(0, Q)$ and $v \sim N(0, R)$, wherein $\boldsymbol{Q} = 0.004 \times \boldsymbol{I}_{8\times 8}$.

Table 2 summarizes some typical component abrupt fault modes and their health parameters deviation from the normal values according to the turbofan engine lab record of Rolls-Royce Company [30].

The performance of the LKF, EKF, and HKF are assessed by four indices, namely, root-mean-square error (*RMSE*), root-mean-square deviation (*RMSD*), convergence time $T_c$, and computational time $T_s$. The *RMSE* and *RMSD* are defined as follows

**TABLE 2. Turbofan engine abrupt fault cases and their deviation magnitudes.**

| Scenarios | Deviation | Component fault modes |
|---|---|---|
| Case 1 | -1% on $SE_1$ | Fan abrupt fault |
| Case 2 | -0.5% on $SE_1$, -1% on $SW_1$ | |
| Case 3 | -1% on $SE_2$ | HPC abrupt fault |
| Case 4 | -1% on $SW_2$ | |
| Case 5 | -1% on $SE_3$ | HPT abrupt fault |
| Case 6 | +1% on $SW_3$ | |
| Case 7 | -1% on $SE_4$ | LPT abrupt fault |
| Case 8 | -0.6% on $SE_4$, +1% on $SW_4$ | |

$$\begin{aligned} RMSE &= [\frac{1}{S}\sum_{i=1}^{S}(\hat{\boldsymbol{x}}_i - \boldsymbol{x}_i)^2]^{\frac{1}{2}} \\ RMSD &= [\frac{1}{S}\sum_{i=1}^{S}(\hat{\boldsymbol{x}}_i - \bar{\hat{\boldsymbol{x}}}_i)^2]^{\frac{1}{2}} \end{aligned} \quad (24)$$

where $S$ is total sampling steps, and $\bar{\hat{x}}_i$ is the mean of estimate value. The convergence time $T_c$ denotes the consuming step to fault recognition, and it is from the staring deviation to the estimate steady state within $\pm 2\%$ range and no longer out of this range in two consecutive steps. The computational time $T_s$ is the total consuming time in a particular simulation.

According to linear correlation analysis, two spool speeds $N_L$, $N_H$, and two temperatures $T_{22}$, $T_3$ separately form two sensor subsets for the local LKFs. The rest sensed data are utilized for the local EKFs, and they are partitioned based on the neighborhood of engine component. Hence, the measurements of five local filters can be denoted by $y_1 = [N_L, N_H]$, $y_2 = [T_{22}, T_3]$, $y_3 = [P_{22}, P_3]$, $y_4 = [T_{43}, P_{43}]$, $y_5 = [T_6, P_6]$, where $y_1$ and $y_2$ are coped by the LKFs, $y_3$, $y_4$ and $y_5$ are by the EKFs.

### A. ESTIMATION ACCURACY FOR ENGINE HEALTH MONITORING

The turbofan engine health estimation tests on abrupt anomaly are carried out at three operation conditions: ground point 1 ($H = 0$m, $Ma = 0$, $W_f = 2.48$kg/s), the operating point 2 ($H = 8000$m, $Ma = 0.5$, $W_f = 1.5$kg/s), and the operating point 3 ($H = 11000$m, $Ma = 0.8$, $W_f = 0.7$kg/s). The sudden shifts of health parameters summarized in Table 2 are added to their normal values at $t = 2$s. Monte Carl simulation implements, and each case runs twenty times. The $T_s$ is the sum of the CPU processing time of local filter and master filter, and the first part is equal to that of the largest consuming time of local filters. The results of abrupt monitoring are reported numerically at different conditions in Table 3.

As shown in Table 3, both the EKF and HKF outperform the LKF in terms of *RMSE* and *RMSD*, while they consume more CPU processing time than the LKF. The estimation quality performed by LKF is relatively poor due to

**TABLE 3.** Estimation performance of the examined filters in abrupt anomaly cases at different conditions.

| Operating Condition | Fault Mode | *RMSE* | | | *RMSD* | | | *Ts* | | |
|---|---|---|---|---|---|---|---|---|---|---|
| | | LKF | EKF | HKF | LKF | EKF | HKF | *LKF* | *EKF* | *HKF* |
| Ground operation 1 | Case 1 | 0.0397 | 0.0228 | 0.0230 | 0.0162 | 0.0196 | 0.0198 | 0.0590 | 0.0881 | 0.0882 |
| | Case 2 | 0.0396 | 0.0225 | 0.0235 | 0.0160 | 0.0192 | 0.0195 | 0.0589 | 0.0877 | 0.0886 |
| | Case 3 | 0.0378 | 0.0233 | 0.0238 | 0.0160 | 0.0196 | 0.0198 | 0.0592 | 0.0880 | 0.0878 |
| | Case 4 | 0.0385 | 0.0242 | 0.0248 | 0.0162 | 0.0197 | 0.0198 | 0.0590 | 0.0882 | 0.0871 |
| | Case 5 | 0.0367 | 0.0240 | 0.0234 | 0.0163 | 0.0199 | 0.0201 | 0.0588 | 0.0879 | 0.0878 |
| | Case 6 | 0. 0356 | 0.0246 | 0.0254 | 0.0160 | 0.0196 | 0.0197 | 0.0583 | 0.0882 | 0.0881 |
| | Case 7 | 0.0368 | 0.0228 | 0.0233 | 0.0160 | 0.0195 | 0.0197 | 0.0586 | 0.0879 | 0.0880 |
| | Case 8 | 0.0380 | 0.0235 | 0.0248 | 0.0160 | 0.0193 | 0.0194 | 0.0584 | 0.0878 | 0.0884 |
| Operating point 2 | Case 1 | 0.0381 | 0.0243 | 0.0249 | 0.0185 | 0.0212 | 0.0222 | 0.0589 | 0.0877 | 0.0880 |
| | Case 2 | 0.0409 | 0.0240 | 0.0243 | 0.0188 | 0.0212 | 0.0216 | 0.0579 | 0.0879 | 0.0883 |
| | Case 3 | 0.0410 | 0.0257 | 0.0269 | 0.0185 | 0.0204 | 0.0217 | 0.0591 | 0.0881 | 0.0879 |
| | Case 4 | 0.0419 | 0.0261 | 0.0258 | 0.0189 | 0.0214 | 0.0212 | 0.0588 | 0.0880 | 0.0874 |
| | Case 5 | 0.0350 | 0.0248 | 0.0252 | 0.0184 | 0.0219 | 0.0214 | 0.0587 | 0.0879 | 0.0877 |
| | Case 6 | 0.0388 | 0.0247 | 0.0253 | 0.0185 | 0.0211 | 0.0210 | 0.0584 | 0.0881 | 0.0881 |
| | Case 7 | 0.0355 | 0.0244 | 0.0244 | 0.0182 | 0.0219 | 0.0223 | 0.0585 | 0.0879 | 0.0881 |
| | Case 8 | 0.0401 | 0.0262 | 0.0260 | 0.0184 | 0.0218 | 0.0223 | 0.0594 | 0.0876 | 0.0883 |
| Operating point 3 | Case 1 | 0.0406 | 0.0298 | 0.0299 | 0.0234 | 0.0251 | 0.0260 | 0.0584 | 0.0879 | 0.0881 |
| | Case 2 | 0.0479 | 0.0288 | 0.0299 | 0.0227 | 0.0256 | 0.0265 | 0.0578 | 0.0877 | 0.0882 |
| | Case 3 | 0.0490 | 0.0287 | 0.0308 | 0.0214 | 0.0257 | 0.0249 | 0.0581 | 0.0881 | 0.0879 |
| | Case 4 | 0.0442 | 0.0305 | 0.0306 | 0.0220 | 0.0260 | 0.0254 | 0.0584 | 0.0883 | 0.0876 |
| | Case 5 | 0.0414 | 0.0300 | 0.0318 | 0.0217 | 0.0255 | 0.0259 | 0.0585 | 0.0878 | 0.0878 |
| | Case 6 | 0.0478 | 0.0291 | 0.0316 | 0.0220 | 0.0247 | 0.0258 | 0.0584 | 0.0880 | 0.0882 |
| | Case 7 | 0.0503 | 0.0295 | 0.0297 | 0.0217 | 0.0246 | 0.0249 | 0.0585 | 0.0882 | 0.0880 |
| | Case 8 | 0.0501 | 0.0290 | 0.0309 | 0.0236 | 0.0248 | 0.0258 | 0.0584 | 0.0878 | 0.0883 |

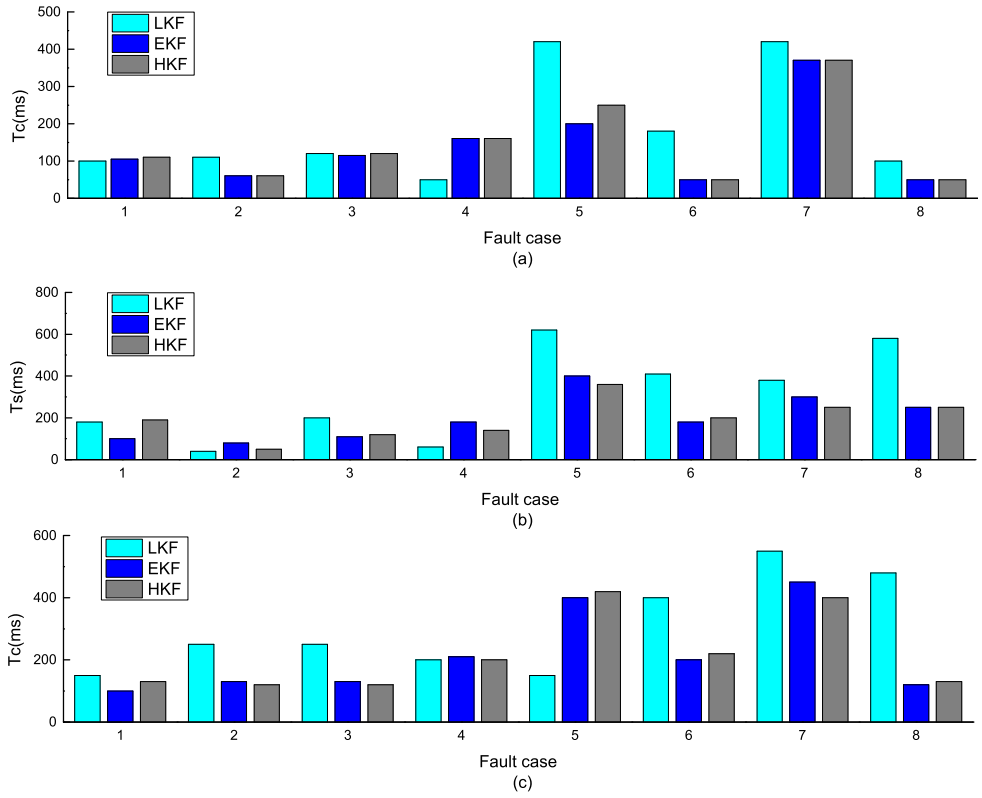


**FIGURE 2.** Convergence time of the examined KFs in engine abrupt deviation cases. (a) Ground operating 1. (b) Operating point 2. (c) Operating point 3.

linearization errors of the modeling. The EKF achieves better estimation accuracy due to its nonlinear characteristics. Since the HKF employs three local EKFs to handle the system nonlinearity, it has a similar level of accuracy as the EKF. Figure 2 gives the convergence times $T_c$ by three examined filters, $T_c$ of the HKF approaches to that of the EKF in many involved cases.

In order to further evaluate the proposed HKF performance to track abrupt shift during gradual deterioration during the engine transient behavior. The turbofan engine runs

**TABLE 4.** Computational burden comparison of HKF and EKF with regard to $T_s$(s).

| Fault Mode | HKF | | | | | | | Centralized EKF |
|---|---|---|---|---|---|---|---|---|
| | Local LKF 1 | Local LKF 2 | Local EKF 1 | Local EKF 2 | Local EKF 3 | Master filter | Total time | |
| Case 1 | 0.0132 | 0.0131 | 0.0476 | 0.0467 | 0.0445 | 0.0408 | 0.0884 | 0.1173 |
| Case 2 | 0.0133 | 0.0132 | 0.0466 | 0.0451 | 0.0477 | 0.0410 | 0.0887 | 0.1150 |
| Case 3 | 0.0132 | 0.0133 | 0.0466 | 0.0473 | 0.0442 | 0.0406 | 0.0879 | 0.1184 |
| Case 4 | 0.0132 | 0.0132 | 0.0465 | 0.0462 | 0.0476 | 0.0405 | 0.0881 | 0.1142 |
| Case 5 | 0.0132 | 0.0133 | 0.0477 | 0.0483 | 0.0465 | 0.0406 | 0.0889 | 0.1182 |
| Case 6 | 0.0131 | 0.0133 | 0.0461 | 0.0470 | 0.0475 | 0.0408 | 0.0883 | 0.1174 |
| Case 7 | 0.0131 | 0.0132 | 0.0462 | 0.0472 | 0.0464 | 0.0407 | 0.0879 | 0.1132 |
| Case 8 | 0.0132 | 0.0131 | 0.0466 | 0.0460 | 0.0471 | 0.0406 | 0.0877 | 0.1155 |
| Average | 0.0132 | 0.0132 | 0.0467 | 0.0467 | 0.0464 | 0.0407 | 0.0882 | 0.1162 |

as follows: $W_f$ linearly decelerates from 2.48 kg/s to 2.28 kg/s, and $A_8$ keeps to 0.2597. Gradual deterioration is that all health parameters move from their normal values to the degradation terminals in 10s with linear trajectories [30]. Eight health parameters equal to 1 at t = 0s, and the degeneration at the end of the sequence at $t = 10$s are set as: $-2.18\%$ on $SE_1$, $-2.85\%$ on $SW_1$, $-6.71\%$on $SE_2$, $-8.99\%$ on $SW_2$, $-3.22\%$ on $SE_3$, $2.17\%$ on $SW_3$, $-0.81\%$ on $SE_4$ and $0.34\%$ on $SW_4$. Two abrupt deviation, $-1\%$ on $SW_1$ and $-1\%$ on $SE_3$ are injected at 5s. A comparison of the examined filters for engine health tracking is depicted in Fig. 3, where the dotted lines and solid lines represent the real and estimated health parameters, respectively.

It can be found from Fig. 3 that the EKF has the best tracking capability, followed by the HKF, and the LKF is the worst one. The *RMSE*s by the examined filters are calculated, and they are separately 0.0884 by the LKF, 0.0234 by the EKF, and 0.0338 by the HKF. The deviation from the real degraded condition is resulted from that the SVM used by LKF is only an approximation of the real turbofan engine with single health parameter degraded. What's more, the mismatch between the linearized model and actual engine increases because of operating point variation. The Jacobian matrix is updated when the operation changes, the EKF tracking performance won't be affected.

### B. COMPUTATIONAL EFFORTS AND ROBUST TO SENSOR FAULT

To demonstrate the reduction of computational effort of the HKF, the $T_s$ in case of turbofan engine abrupt fault diagnosis is tested. Since the HKF performs in the distributed architecture and local filters run in parallel, the $T_s$ is the sum of the running time of local filters and master filter, and the running time of local filters is equal to the longest one among local filters. Table 4 shows the $T_s$ of HKF and EKF in eight abrupt fault cases.

In Table 4, the average computation time of master filter is about 0.0407s, and those of local LKF and local EKF are 0.0132s and 0.046s, respectively. The average time of HKF in eight abrupt anomaly modes is 0.882 while that of EKF is 0.1162s. Compared to the EKF, the HKF reduces the computational time by 0.028s (24.1%). The computational burden is relieved because of the dispersed structure of HKF. The centralized KFs afford the whole computing process only by one processor, while it is assigned to five local filters and one master filter in the HKF.

Sensor failure is another important challenge for the reliability of engine health monitoring. In order to evaluate the robustness of the HKF to sensor fault, estimation simulations are carried out with the sensor step fault and impulse fault cases. A comparison of the HKF and EKF is presented at ground design point. Gas turbine engine experiences gradual degradation with a step fault 3% on sensor $T_3$ at 5s is simulated in Fig. 4.

As it can be observed from Fig. 4, both of the EKF and HKF can track the engine performance degradation before the step fault is injected to compressor exit temperature sensor $T_3$. There is a large deviation between the true health parameters and their estimates generated by the EKF after 5s. In particular, the compressor efficiency $SE_2$ and the HPT efficiency $SE_3$ have about 6% deviation. In contrast, the estimates by the HKF follow the actual performance deterioration curve all the time. Likewise, the test of engine gradual degradation with sensor impulse fault is carried out at ground operation.

The sensor robustness simulation results indicate that the estimates by the centralized EKF are easily polluted once sensor failure occurs. That is to say, the EKF in the centralized structure is unable to self-tune and isolate the faulty sensor. Compared to the centralized EKF, the HKF has better robust to sensor step and impulse fault in virtue of the number and weight of local KFs change. Therefore, the HKF can readily perform engine health estimation with the capability of sensor fault tolerance.

### C. HKF WITH ASYNCHRONOUS FUSION MECHANISM SIMULATION

It is noteworthy that the computational time of each local estimator is usually different in the distributed structure, and the simulation of asynchronous HKF is performed in this section. Let the time consumption of calculation in the local EKFs equal to 60 ms, and that in the local LKFs equal to 20 ms. The asynchronous fusion mechanism is utilized in the

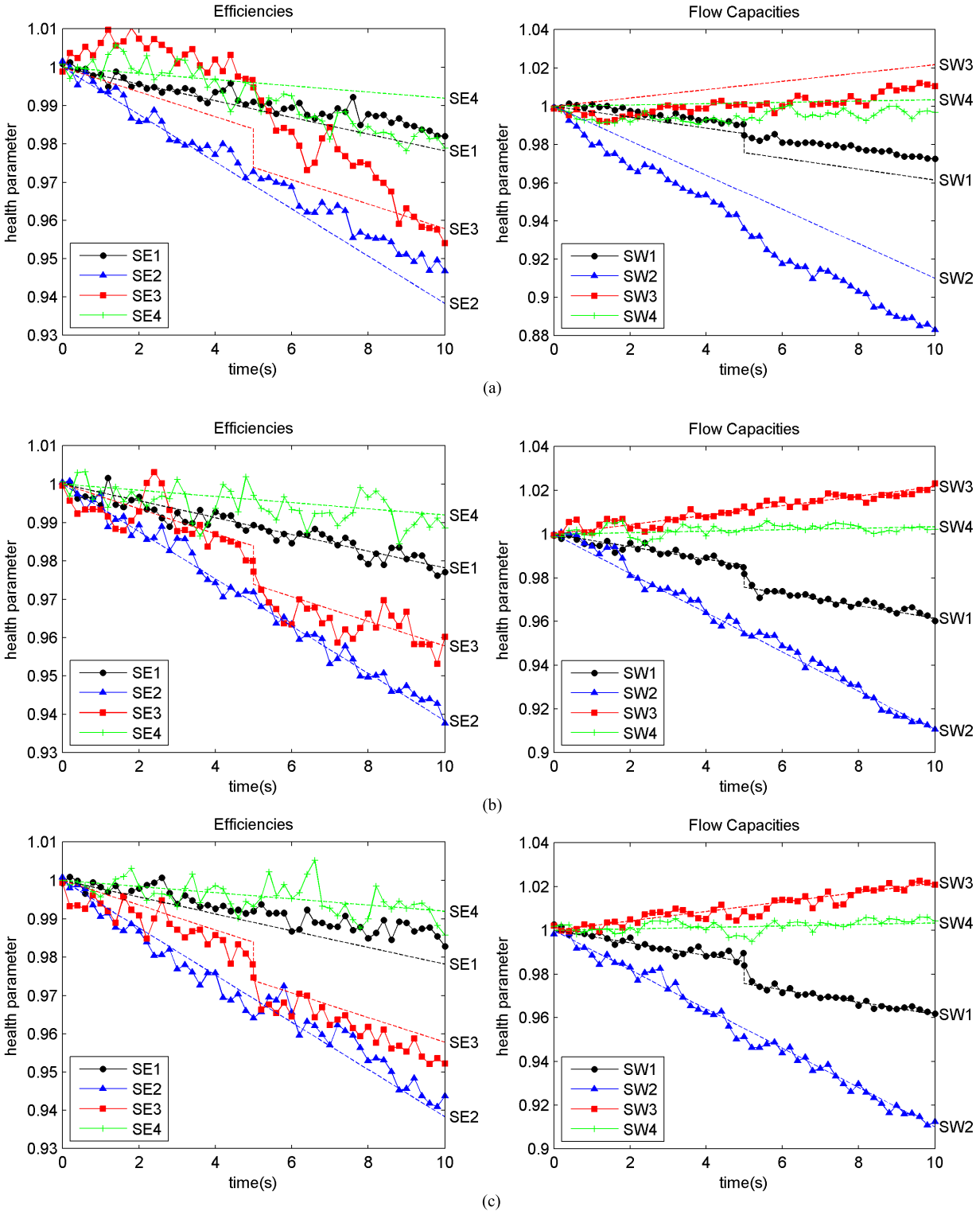


**FIGURE 3.** Gas turbine engine performance tracking under dynamic operation. (a) LKF. (b) EKF. (c) HKF.

HKF (denoted by the AHKF), and it is assessed at ground operation point. The results of engine health monitoring by the AHKF in the cases of mixed gradual deterioration and abrupt deviation ($-1\%$ on $SE_3$ and $-1\%$ on $SW_1$) are depicted in Fig. 5.

From Fig. 5, the AHKF can track engine performance degradation precisely. *RMSE* by the HKF with asynchronous fusion mechanism simulation is 0.0304, while *RMSE* by the HKF in simultaneously computation of the local KFs is 0.0275. It follows that the asynchronous fusion

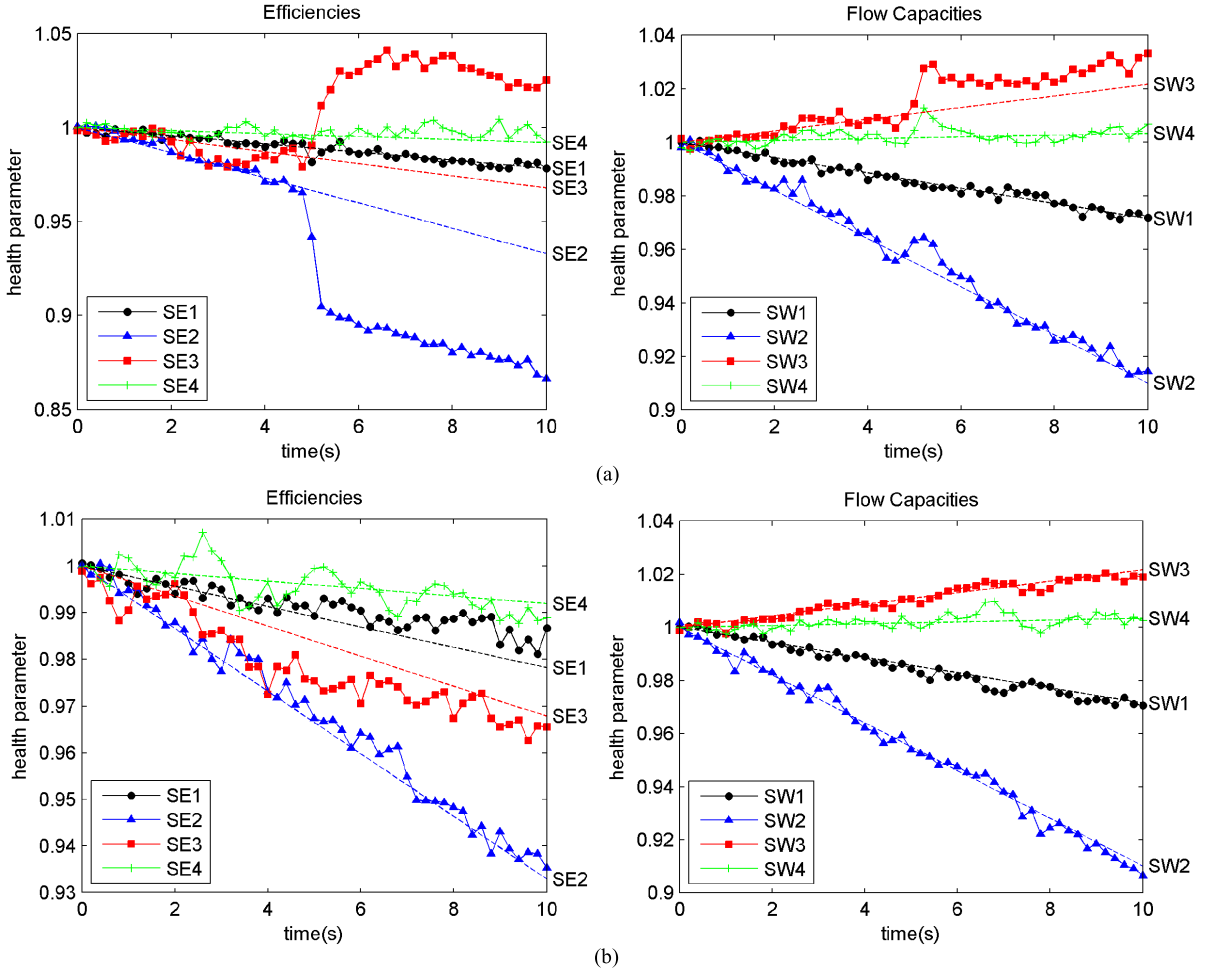


**FIGURE 4.** Gas turbine engine health monitoring with 3% step fault on sensor $T_3$. (a) EKF. (b) HKF.

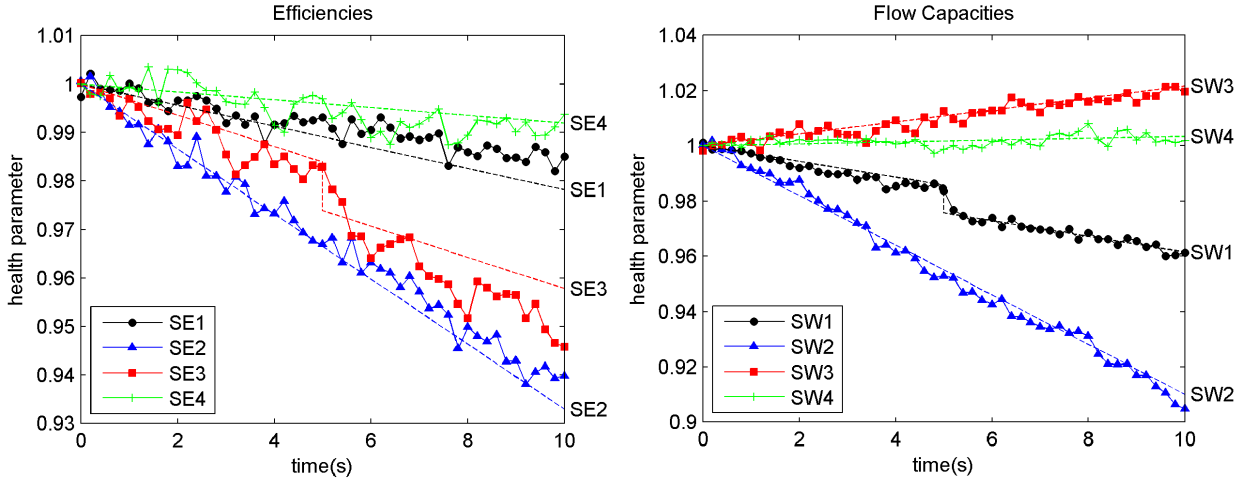


**FIGURE 5.** Asynchronous fusion estimation performance under abrupt deviation with gradual deterioration by the AHKF.

mechanism of the HKF has a little slow response to abrupt deviation. In order to further illustrate the performance of the HKF with asynchronous fusion mechanism, the engine abrupt deviation in Table 2 are tested at ground operation and each case is performed for twenty times. A comparison of HKF with asynchronous computation in eight abrupt fault cases with regards to *RMSE*, *RMSD* and $T_c$ are reported in Table 5.

**TABLE 5. The estimation performance of asynchronous HKF in the cases of engine abrupt deviation.**

| Fault | *RMSE* | | *RMSD* | | $T_c$(ms) | |
|---|---|---|---|---|---|---|
| Modes | HKF | AHKF | HKF | AHKF | HKF | AHKF |
| Case 1 | 0.0233 | 0.0247 | 0.0199 | 0.0211 | 108 | 126 |
| Case 2 | 0.0231 | 0.0240 | 0.0197 | 0.0210 | 60 | 156 |
| Case 3 | 0.0261 | 0.0269 | 0.0197 | 0.0211 | 188 | 262 |
| Case 4 | 0.0247 | 0.0254 | 0.0194 | 0.0214 | 346 | 464 |
| Case 5 | 0.0253 | 0.0269 | 0.0198 | 0.0212 | 328 | 362 |
| Case 6 | 0.0267 | 0.0275 | 0.0197 | 0.0206 | 79 | 204 |
| Case 7 | 0.0238 | 0.0242 | 0.0202 | 0.0207 | 305 | 400 |
| Case 8 | 0.0242 | 0.0249 | 0.0196 | 0.0206 | 45 | 128 |

Table 5 shows that the biggest difference in *RMSE*s by the HKF and AHKF is less than 0.0016, and that in *RMSD*s is also less than 0.0014. The estimation accuracy is hardly affected by the consuming time difference of local processors as the asynchronous fusion mechanism is used in the HKF. While it can be clearly found that the convergence time $T_c$ of these involved HKFs produces a certain gap in all fault cases, $T_c$ increases are owing to the longer output cycle of local EKFs in the AHKF. It reveals that the HKF with the asynchronous fusion mechanism has satisfactory estimation accuracy, on the premise of ensuring periodic output of global estimation.

## V. CONCLUSION

This paper proposes a hybrid fusion filtering approach based on federated filtering technique for gas turbine engine health monitoring. Compared to general centralized KFs, the improvement of this methodology lies in the integration of the linear and nonlinear KFs to yield an optimal global state estimate in the distributed structure and asynchronous fusion mechanism introduced. The health parameters computational burden is dispersed from one filter processor center to five parallel local filters and one master filter in this distributed architecture. Three local EKFs are utilized to process sensor subsets with strong measurement nonlinearity, and two local LKFs to process the remaining subsets. Several key aspects concerning state estimation robustness to sensor faults, asynchronous fusion mechanism, and equivalence of the HKF and centralized EKF are mathematically discussed in this paper.

This approach is evaluated under various engine health anomalies involving abrupt deviation, gradual deterioration and their mixtures. The engine health estimation tests are performed under three conditions: the steady behavior at ground and high-altitude points, and the dynamic behavior. The simulation results demonstrate that one advantage of the proposed HKF has less computational burden than the centralized EKF, which brings the benefits of real time on-board implement of engine health estimation. The other advantage of this approach is robust to step fault and impulse fault on sensors according to the simulations on sensor fault tolerance. In addition, the asynchronous fusion mechanism is given in HKF, and the results show the HKF performs well even output cycles of local KFs are inconsistent.

This research presents a distributed filtering methodology by combining linear and nonlinear KFs, which is particularly advantageous for gas turbine engine health monitoring. However, several important aspects related to this work can be explored in our future research. First, health parameters to be estimated are the same in every local filter, and it would be interesting to discuss how the proposed method perform when each local filter devotes to estimate a different subspace of the state variables. Second, the evaluation of the HKF for engine health estimation is limited to the numerical simulation, and it will be of more practical significance to examine these involved filtering methodologies based on the experiments on semi-physical hardware in loop simulation.

## ACKNOWLEDGEMENTS

The authors would like to thank the anonymous reviewers for their constructive comments and great help in the writing process, which will improve the manuscript significantly.

## REFERENCES

[1] A. J. Volponi, "Gas turbine engine health management: Past, present, and future trends," *J. Eng. Gas Turbines Power*, vol. 136, no. 5, p. 051201, 2014.
[2] M. A. Zaidan, A. R. Mills, R. F. Harrison, and P. J. Fleming, "Gas turbine engine prognostics using Bayesian hierarchical models: A variational approach," *Mech. Syst. Signal Process.*, vols. 70–71, pp. 120–140, Mar. 2016.
[3] N. Zhao, X. Wen, and S. Li, "A review on gas turbine anomaly detection for implementing health management," in *Proc. ASME Turbo Expo, Turbomachinery Tech. Conf. Expo.*, Seoul, South Korea, Jun. 2016, p. V001T22A009.
[4] J. Kraft, V. Sethi, and R. Singh, "Optimization of aero gas turbine maintenance using advanced simulation and diagnostic methods," *J. Eng. Gas Turbines Power*, vol. 136, no. 11, p. 111601, 2014.
[5] D. L. Simon and J. B. Armstrong , "An integrated approach for aircraft engine performance estimation and fault diagnostics," *J. Eng. Gas Turbines Power*, vol. 135, no. 7, p. 071203, 2013.
[6] X. Pu, S. Liu, H. Jiang, and D. Yu, "Adaptive gas path diagnostics using strong tracking filter," *Proc. Inst. Mech. Eng. G, J. Aerosp. Eng.*, vol. 228, no. 4, pp. 577–585, 2014.
[7] X. Yan, M. Jia, and L. Xian, "Compound fault diagnosis of rotating machinery based on OVMD and a 1.5-dimension envelope spectrum," *Meas. Sci. Technol.*, vol. 27, no. 7, p. 075002, 2016.
[8] C. Lin and V. Makis, "Application of vector time series modeling and T-squared control chart to detect early gearbox deterioration," *Int. J. Performability Eng.*, vol. 10, no. 1, pp. 105–114, 2014.
[9] S. Kiakojoori and K. Khorasani, "Dynamic neural networks for gas turbine engine degradation prediction, health monitoring and prognosis," *Neural Comput. Appl.*, vol. 27, no. 8, pp. 2157–2192, 2016.
[10] S. Sampath and R. Singh, "An integrated fault diagnostics model using genetic algorithm and neural networks," *J. Eng. Gas Turbines Power*, vol. 128, no. 1, pp. 49–56, 2006.
[11] C. Yang, X. Kong, and X. Wang, "Model-based fault diagnosis for performance degradations of turbofan gas path via optimal robust residuals," in *Proc. ASME Turbo Expo Turbomach. Tech. Conf. Expo.*, Seoul, South Korea, Jun. 2016, p. V006T05A004.
[12] S. Zhong, X. Xie, L. Lin, and F. Wang, "Genetic algorithm optimized double-reservoir echo state network for multi-regime time series prediction," *Neurocomputing*, vol. 238, pp. 191–204, May 2017.
[13] D. Simon, "A comparison of filtering approaches for aircraft engine health estimation," *Aerosp. Sci. Technol.*, vol. 12, no. 4, pp. 276–284, 2008.
[14] S. Roy, R. H. Hashemi, and A. J. Laub, "Square root parallel Kalman filtering using reduced-order local filters," *IEEE Trans. Aerosp. Electron. Syst.*, vol. 27, no. 2, pp. 276–289, Mar. 1991.
[15] N. A. Carlson, "Federated square root filter for decentralized parallel processors," *IEEE Trans. Aerosp. Electron. Syst.*, vol. 26, no. 3, pp. 517–525, May 1990.
[16] M. Kazerooni and A. Khayatian, "Data fusion for autonomous vehicle navigation based on federated filtering," in *Proc. IEEE Austral. Control Conf. (AUCC)*, Nov. 2011, pp. 368–373.

[17] S. Yang, G. Yang, Z. Zhu, and J. Li, "Stellar refractionŰbased SINS/CNS integrated navigation system for aerospace vehicles," *J. Aerosp. Eng.*, vol. 29, no. 2, p. 04015051, 2015.
[18] X. Gong and J. Zhang, "An innovative transfer alignment method based on federated filter for airborne distributed POS," *Measurement*, vol. 86, pp. 165–181, May 2016.
[19] G. Liu and H. Zhu, "EM-FKF approach to an integrated navigation system," *J. Aerosp. Eng.*, vol. 27, no. 3, pp. 621–630, 2014.
[20] Z. Xing and Y. Xia, "Distributed federated Kalman filter fusion over multisensor unreliable networked systems," *IEEE Trans. Circuits Syst. I, Reg. Papers*, vol. 63, no. 10, pp. 1714–1725, Oct. 2016.
[21] S. Zhang, Y. Guo, and J. Feng, "Design and simulation validation of an integrated on-board aircraft engine diagnostic architecture," *Acta Aeronautica Astronautica Sinica*, vol. 35, no. 2, pp. 381–390, 2014.
[22] H. Wen, Z. H. Zhu, D. Jin, and H. Hu, "Model predictive control with output feedback for a deorbiting electrodynamic tether system," *J. Guid., Control, Dyn.*, vol. 39, no. 10, pp. 2455–2460, 2016.
[23] S. Borguet and O. Léonard, "Comparison of adaptive filters for gas turbine performance monitoring," *J. Comput. Appl. Math.*, vol. 234, no. 7, pp. 2202–2212, 2010.
[24] G. A. Terejanu. *Extended Kalman Filter Tutorial*. [Online]. Available: https://homes.cs.washington.edu/~todorov/courses/cseP590/readings/tutorialEKF.pdf
[25] J. Xu, Y. Wang, and L. Xu, "PHM-oriented sensor optimization selection based on multiobjective model for aircraft engines," *IEEE Sensors J.*, vol. 15, no. 9, pp. 4836–4844, Sep. 2015.
[26] M. Chen, L. Q. Hu, and H. Tang, "An approach for optimal measurements selection on gas turbine engine fault diagnosis," *J. Eng. Gas Turbines Power*, vol. 137, no. 7, p. 071203, 2015.
[27] F. Lu, J. Q. Huang, X. J. Qiu, and Y. D. Xing, "Feature extraction based on information entropy fusion for turbo-shaft engine gas-path analysis," *Chin. J. Sci. Instrum.*, vol. 33, no. 1, pp. 13–19, 2012.
[28] X. L. Huang, H. Q. Lu, and Y. F. Wang, "In coordinate interval federated filtering of integrated navigation," *J. Chin. Inertial Technol.*, vol. 10, no. 3, pp. 1–7, 2002.
[29] Z. Wenxiang, "Research on object-oriented modeling and simulation for aeroengine and control system," Ph.D. dissertation, College Energy Power Eng., Nanjing Univ. Aeronautics Astron., Nanjing, China, 2006.
[30] J. DeCastro, J. Litt, and D. Frederick, "A modular aero-propulsion system simulation of a large commercial aircraft engine," in *Proc. 44th AIAA/ASME/SAE/ASEE Joint Propuls. Conf., Exhib., Joint Propuls. Conf.*, 2008, pp. 1–6, paper NASA/TM-2008-215303.

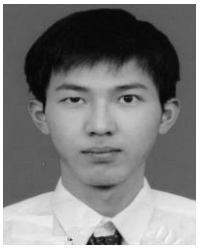

**FENG LU** received the Ph.D. degree in system control and simulation from the Nanjing University of Aeronautics and Astronautics, Nanjing, China, in 2009. From 2012 to 2015, he was with the Aviation Motor Control System Institute as a Post-Doctoral Fellow, where he worked on aircraft engine control system modeling and health monitoring. From 2016 to 2017, he was a Visiting Professor with the Department of Mechanical and Industrial Engineering, University of Toronto. Since 2009, he has been with the College of Energy and Power Engineering, Nanjing University of Aeronautics and Astronautics, first as a Lecturer, and then as an Associate Professor since 2013.

His current research interests are in the fields of gas turbine engine modeling, control, and health prognostics.

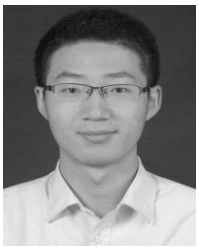

**YIHUAN HUANG** received the master's degree in aerospace propulsion theory and engineering from the Nanjing University of Aeronautics and Astronautics, Nanjing, China, in 2017. Since 2017, he has been with the Aviation Motor Control System Institute, Aviation Industry Corporation of China, as an Engineer.

His current research interests are in the fields of gas turbine engine modeling and health estimation.

**JINQUAN HUANG** received the M.S. and Ph.D. degree in aerospace propulsion system theory and engineering from the Nanjing University of Aeronautics and Astronautics, Nanjing, in 1987 and 1998, respectively. From 1996 to 1997, he was with The University of Texas at Arlington, USA, as a Research Fellow, where he worked on intelligent control and neural networks. Since 1987, he has been with the College of Energy and Power Engineering, Nanjing University of Aeronautics and Astronautics, as an Assistant, a Lecturer, and an Associate Professor, and then a Professor since 1999.

His current research interests are in the fields of gas turbine engine modeling, control, and health management.

**XIAOJIE QIU** received the Ph.D. degree in system control and simulation from the Nanjing University of Aeronautics and Astronautics, Nanjing, China, in 2012. Since 2012, he has been with the Aviation Motor Control System Institute, Aviation Industry Corporation of China, first as an Engineer, and then as a Senior Engineer since 2016.

His current research interests are in the fields of gas turbine engine modeling, control, and health monitoring.